Figure S1A-C. Generation of *Tph2*-deficient mice

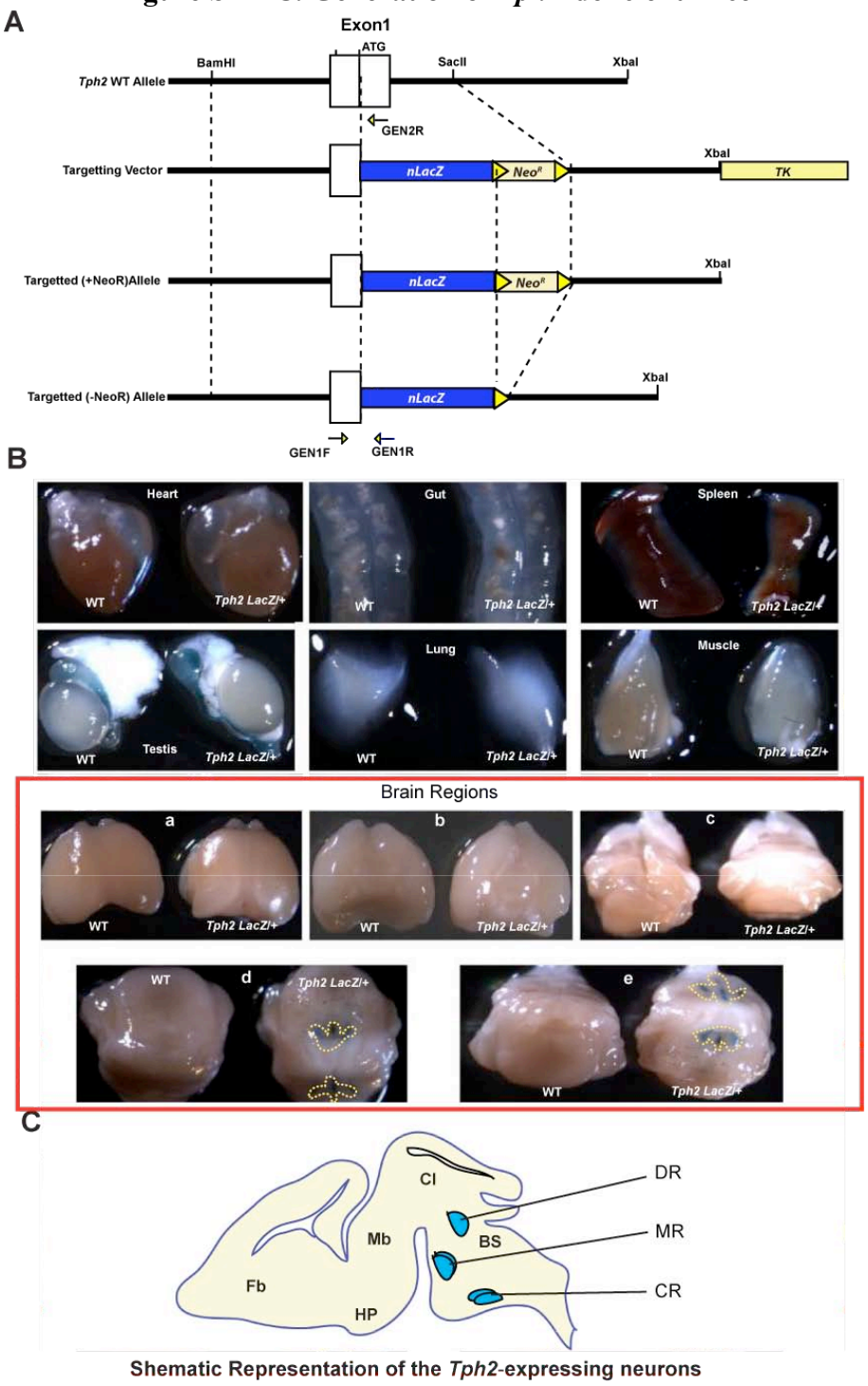

Figure S1. (A) Targeting strategy for generating *Tph2*-/- mice through homologous recombination in embryonic stem (ES) cells. (B) β-galactosidase staining of different tissues of WT (left) and *Tph2*-/- (right) mice brain (a-e) [a: Cerebral cortex (dorsal view); b: Cerebral cortex (ventral view); c: Cerebellum; d and e: Brain stem]. Positive brain areas are highlighted with dotted yellow lines. (C) Schematic representation of locus of β-galactosidase-positive neurons (in blue) in adult mouse brain. DR: dorsal raphe; MR; median raphe; CR: caudal raphe

Figure S1D. Characterization of *Tph2* expression throughout the brain

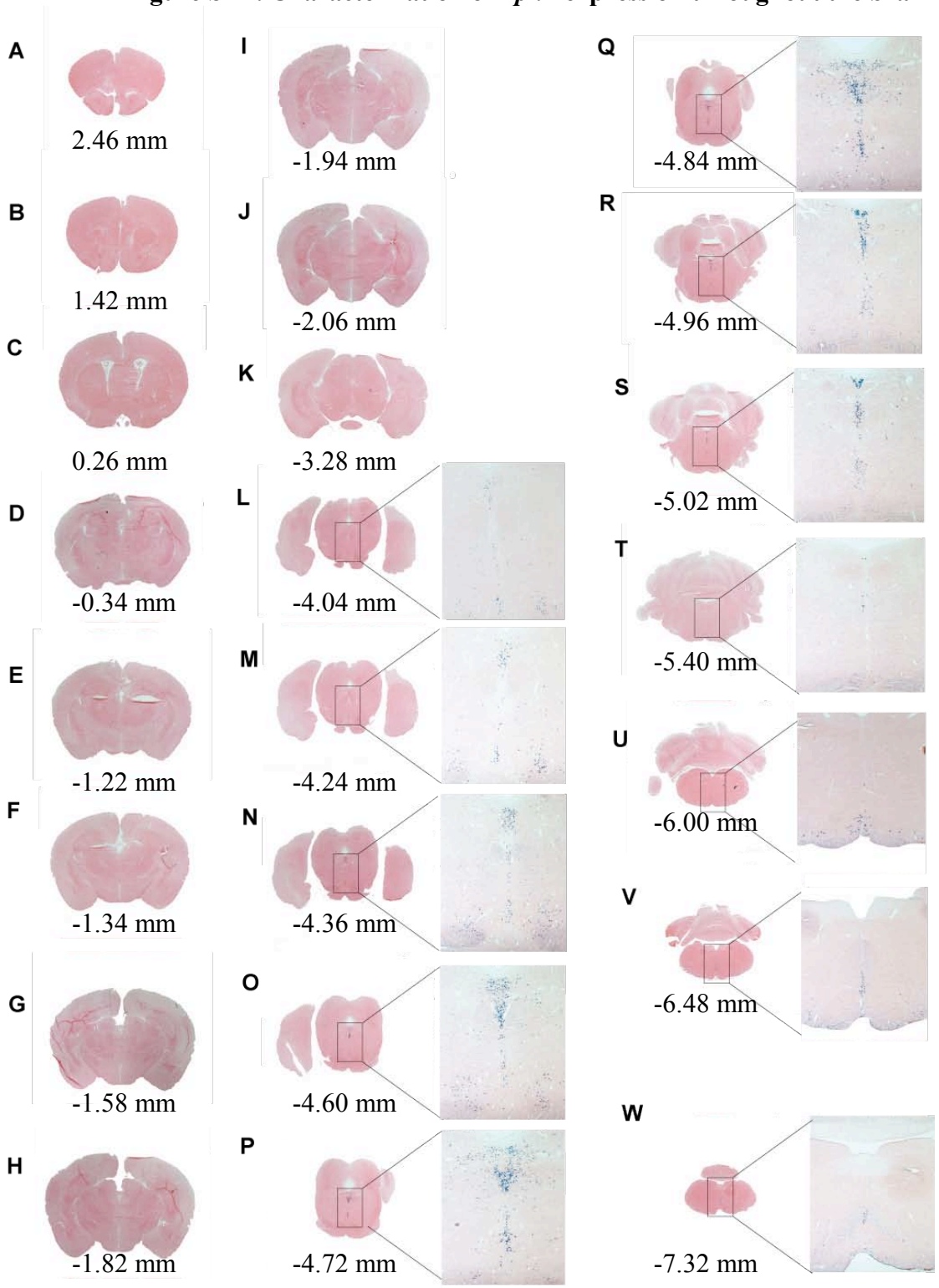

Figure S1D. Series of brain 20 μm cryosections (A-W) from *Tph2*/*LacZ* mice were stained with β-galactosidase at 37°C, counterstained in eosin, cleared and mounted in DPX. Pictures 1X and inset 5X. *Tph2*-positive neurons are in blue. Please note that only brain regions with positive labeling have been shown in the 5X magnification. Bregma locations of sections are indicated below each panel.

Figure S1E. Serum levels of T4 and Corticosterone in *Tph2*-/- mice

	WT	*Tph2*-/-
Serum T4 (ug/dL)	3.09 ± 0.02$^{(n=5)}$	3.00 ± 0.01$^{(n=6)}$
Serum Corticosterone (ng/ml)	181.47 ± 31.09$^{(n=6)}$	221.92 ± 37.05$^{(n=8)}$

Figure S1E. Serum T4 and corticosterone were measured by radio-immunoassay in *Tph2*-/- mice following manufacturers instructions (MP Biomedicals, Corticosterone: Cat#07-120102; T4: Cat#06B-254011)

Figure S2. Bone mineralization is normal in *Tph2*-/- mice.

	WT	*Tph2*-/-
BV/TV%	17.19 ± 1.2$^{(n=4)}$	10.99 ± 1.3$^{(n=4)}$ *
OS/BS	18.99 ± 3.10$^{(n=4)}$	21.12 ± 3.01$^{(n=4)}$

Figure S2. Analysis of non-mineralized bone matrix in *Tph2*-/- mice. Osteoid surface/ bone surface was measured as an indicator of bone mineralization using the Osteomeasure software. Data are presented as Mean ± SEM. * $p<0.05$. Student's t test.

Figure S3A. Changes in Norepinephrine levels in WT and *Tph2*-/- brain.

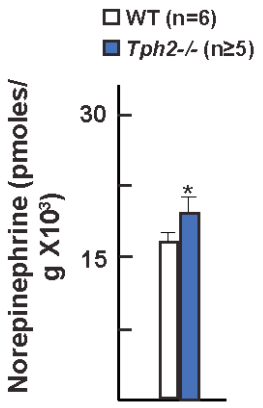

Figure S3A. HPLC analysis of brain norepinephrine levels in WT and *Tph2*-/- brain. * p<0.05 SEM

Figure S3B. Body weight and serum hormone levels in WT and *Tph1*-/-;*Tph2*-/- mice.

	WT	*Tph1*-/-;*Tph2*-/-
Body weight (3 month; gm)	24.11 ± 1.10$^{(n=7)}$	23.15 ± 1.2$^{(n=7)}$
Serum T4 (ug/dL)	3.12 ± 0.12$^{(n=4)}$	3.25 ± 0.21$^{(n=4)}$
Serum Corticosterone (ng/ml)	201.46 ± 30.12$^{(n=4)}$	231.96 ± 27.11$^{(n=4)}$
Plasma Leptin (ng/ml)	3.2 ± 0.7$^{(n=6)}$	3.5 ± 0.4$^{(n=5)}$
Plasma Insulin (ng/ml)	3.8 ± 0.7$^{(n=6)}$	4.4 ± 0.5$^{(n=5)}$
Body Length (cm)	10.91 ± 1.0$^{(n=6)}$	10.12 ± 1.1$^{(n=5)}$

Figure S3B. Body weight analysis, serum T4 and corticosterone, plasma leptin and insulin and body length in 3 month-old WT and *Tph1*-/-;*Tph2*-/- mice. Body weight curve and hormonal changes in *Tph2*-/- has been presented in figure 1H and S1E and S6H. Number of mice used for each of the analysis is indicated in superscript above each value.

Figure S4A. Neuro-anatomical tracing: Surgical site of application for Rhodamine dextran

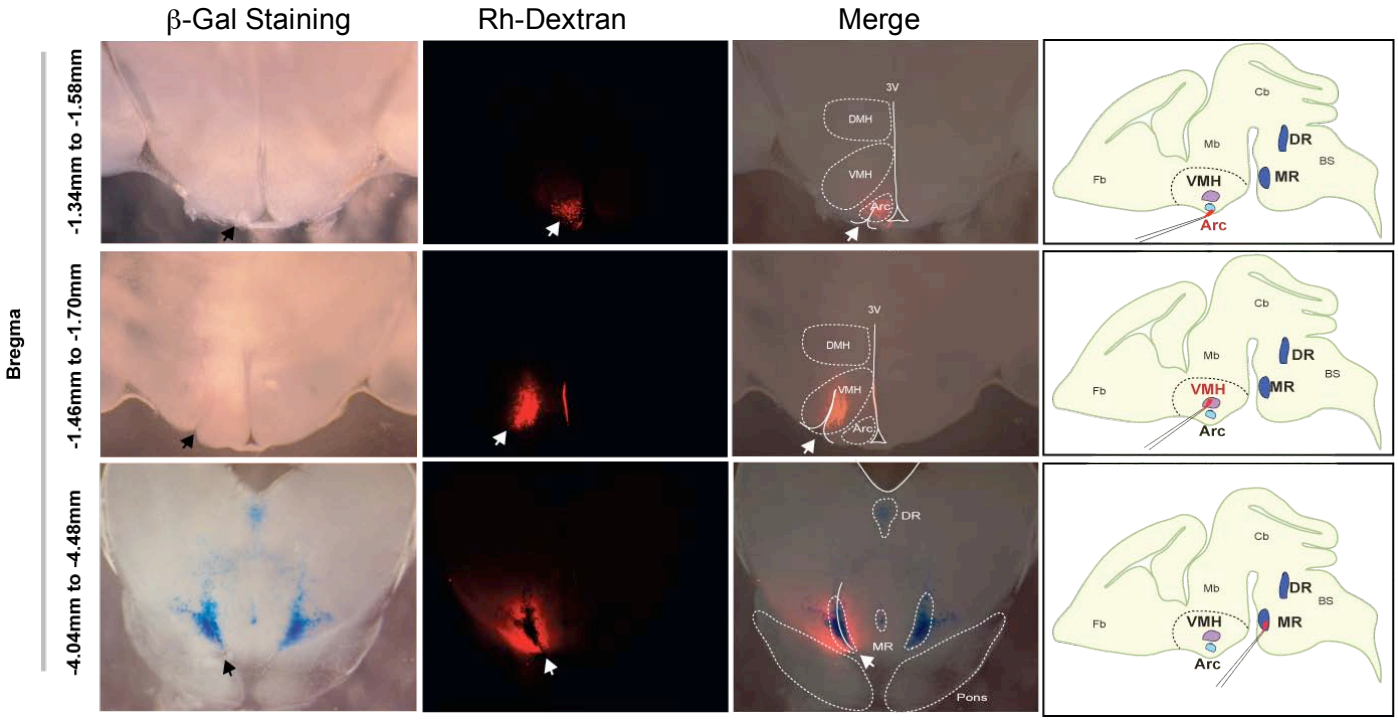

Figure S4A. Rhodamine dextran application sites for arcuate, VMH and median raphe application. Brain section of *Tph2LacZ*/+ mice (200μm) showing rhodamine dextran application sites for arcuate nucleus (A), Ventro medial hypothalamus (B), and median raphe (C). White lines and arrows indicate the exact sites of surgical application of rhodamine dextran. *Tph2*-expressing neurons were revealed by β-galactosidase staining. VMH, DMH and Arc are outlined by dashed line in panels.

Figure S4B. Retrograde Rhodamine-Dextran tracing

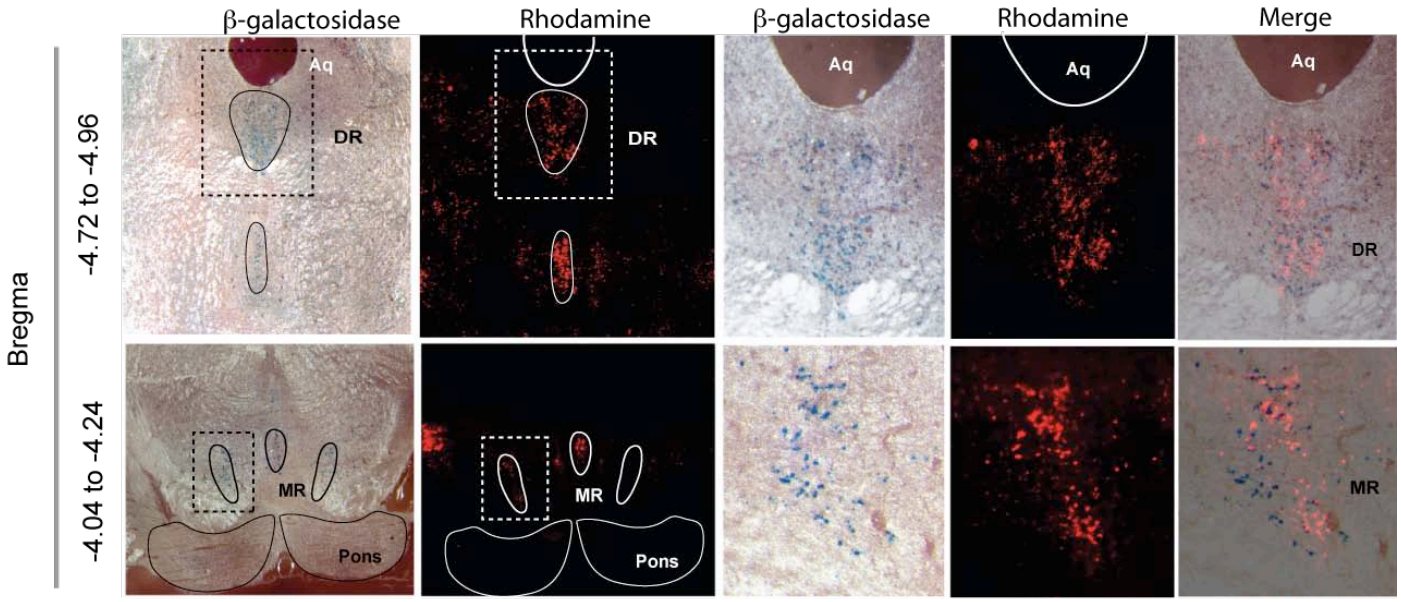

Figure S4B. Rhodamine-Dextran retrograde tracing. After arcuate (Top panel) and VMH (Bottom panel) application of Rhodamine dextran in *Tph2LacZ*/+ mice brains, coronal sections (40-50μm) were prepared through the dorsal raphe (Top panel) and median raphe (Bottom panel) and stained with β-gal or visualized for Rhodamine dextran demonstrating that these neurons project respectively to the Arcuate and VMH neurons. *Tph2*-expressing neurons are revealed by β-galactosidase staining and Rhodamine dextran images show the projections and cell body of the neurons.

Figure S4C. In situ hybridization of *Htr2c* and *Pomc1*

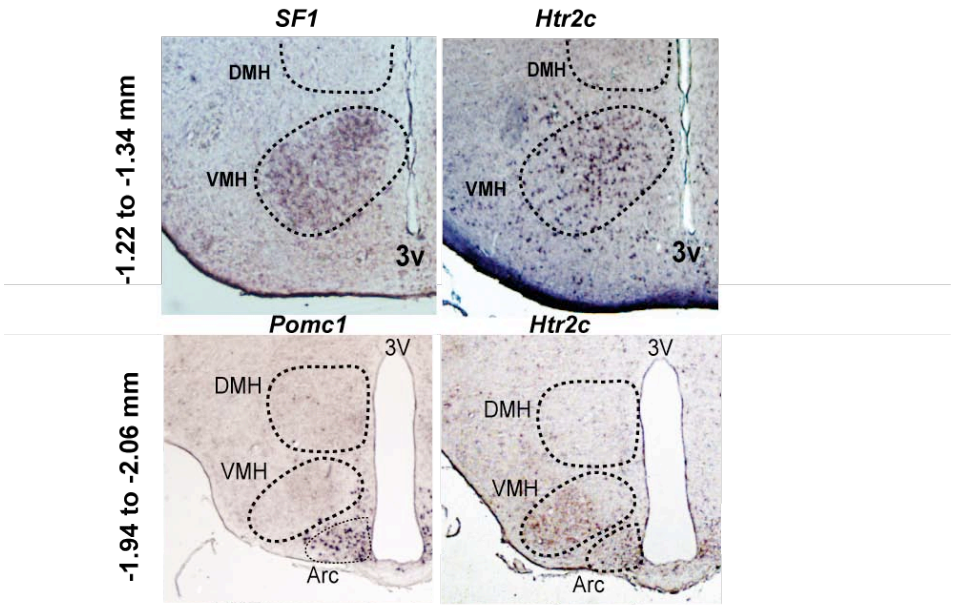

Figure S4C. Cross-sections through the VMH and Arcuate (Arc) hypothalamus in WT mice. In situ hybridization analysis of *Htr2c* expression in VMH and arcuate nuclei in comparison to *Sf1* and *Pomc-1* expression on adjacent sections.

Figure S4D-H. Analysis of *Htr2c*-/- mice

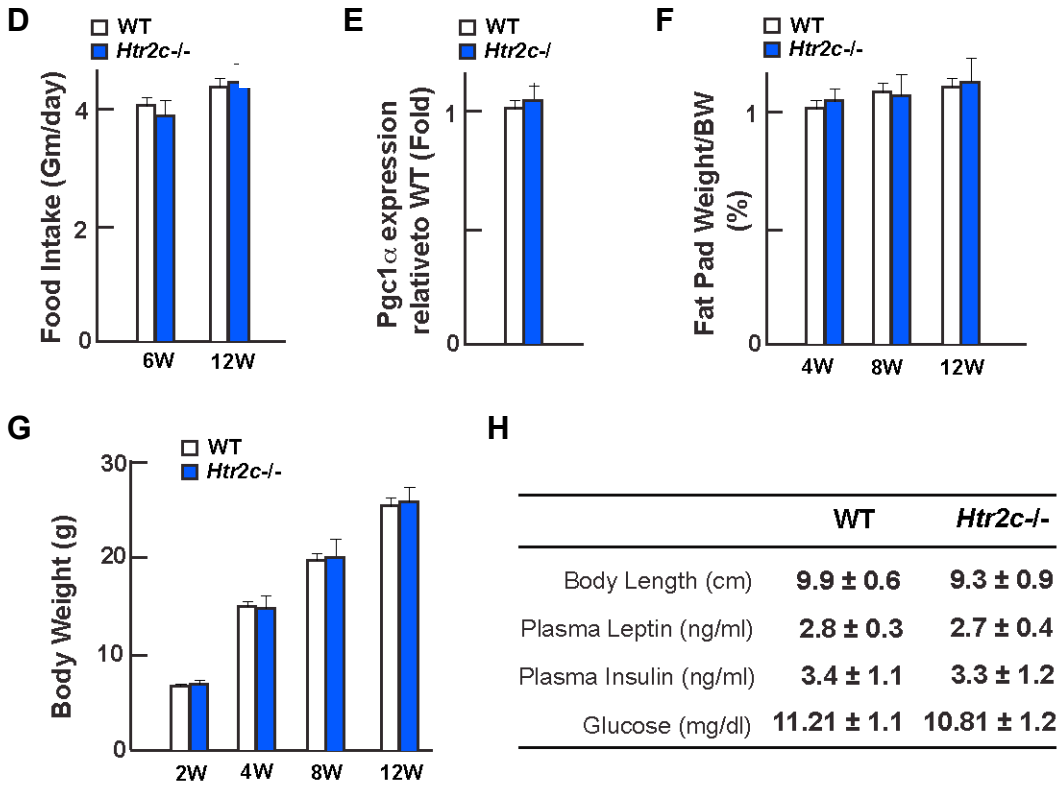

H

	WT	*Htr2c-/-*
Body Length (cm)	**9.9 ± 0.6**	**9.3 ± 0.9**
Plasma Leptin (ng/ml)	**2.8 ± 0.3**	**2.7 ± 0.4**
Plasma Insulin (ng/ml)	**3.4 ± 1.1**	**3.3 ± 1.2**
Glucose (mg/dl)	**11.21 ± 1.1**	**10.81 ± 1.2**

Figure S4 (D-H) Food intake (D), *Pgc1α* expression in brown adipose tissue (E), fat pad weights (F) and body weight analysis (G) in WT and *Htr2c*-/- mice at indicated ages. Changes in body length plasma leptin, insulin and blood glucose levels in WT and *Htr2c*-/- mice at 3 months of age (H).

Figure S4I. Western blot analysis of serotonin receptors in the hypothalamus

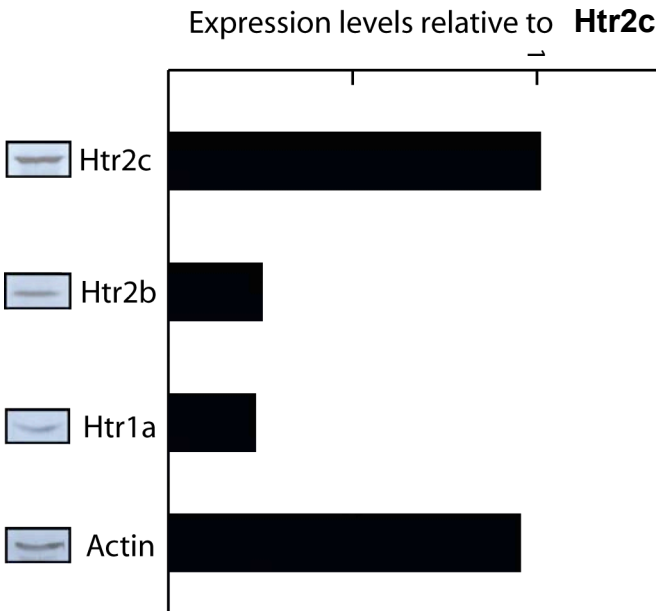

Figure S4I. Western blot analysis of serotonin receptors in hypothalamus. 100 μg of hypothalamus lysate prepared from WT mice were elctrophoresed on SDS-PAGE, blotted on PVDF/nitrocellulose membrane and were probed with antibodies against Htr2c, Htr2b, Htr1a and actin.

Figure S4J. ***Htr2c*** **re-expression in mice**

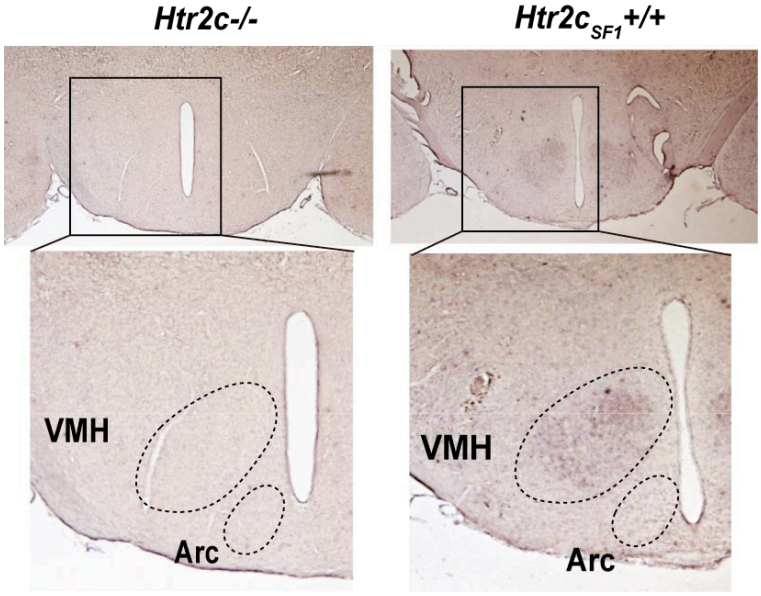

Figure S4J. In situ hybridization analysis of *Htr2c*-/- and *Htr2c* re-expression in ventromedial hypothalamus using *Sf1-Cre* mice**.**

Figure S5. Ucp1 expression in brown adipose tissue

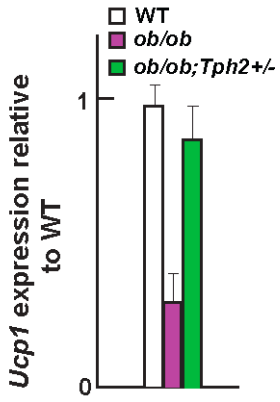

Figure S5. Real-time PCR analysis of *Ucp1* expression in brown adipose tissue in WT, ob/ob and *ob*/*ob*;*Tph2*+/- mice at 3 months of age. $p<0.05$, SEM

Figure S6A-B. Glucose metabolism in *Tph2*-/- mice

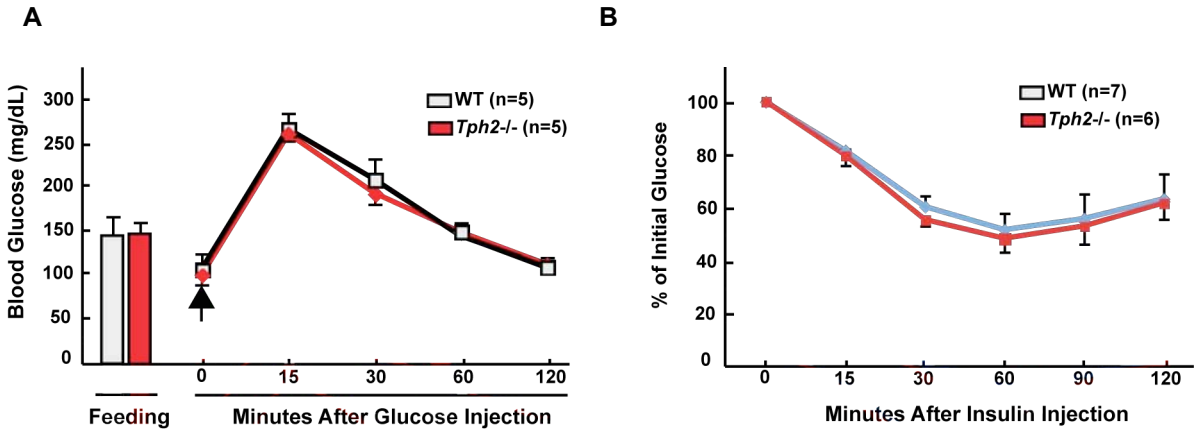

Figure S6A-B. Feeding blood glucose levels (A) Glucose tolerance (A) and insulin tolerance (B) tests in 3-month-old WT and *Tph2*-/- mice.

Figure S6C. MTII-induced changes in cFos expression in WT and *Tph2*-/- hypothalamus

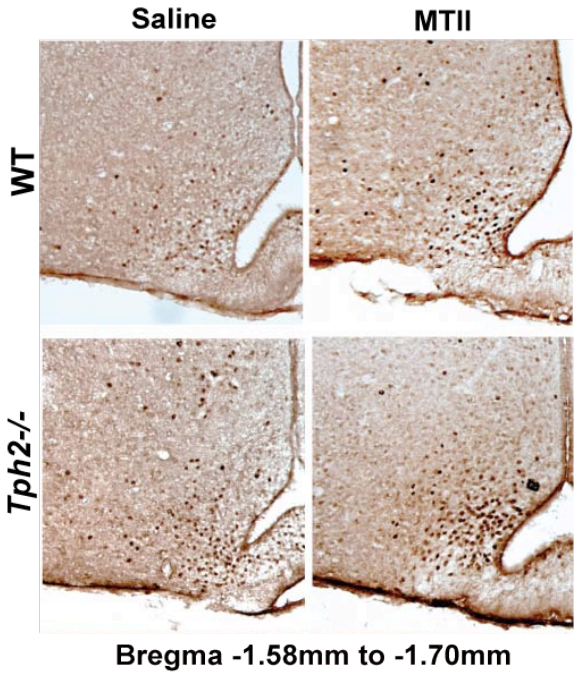

Figure S6C. MTII-induced changes in cFos expression in WT and *Tph2*-/- hypothalamus as described in supplemental methods section

Figure S6D-G. Energy Expenditure analysis in *Htr1a*-/- and *Htr2b*$_{POMC}$-/- mice

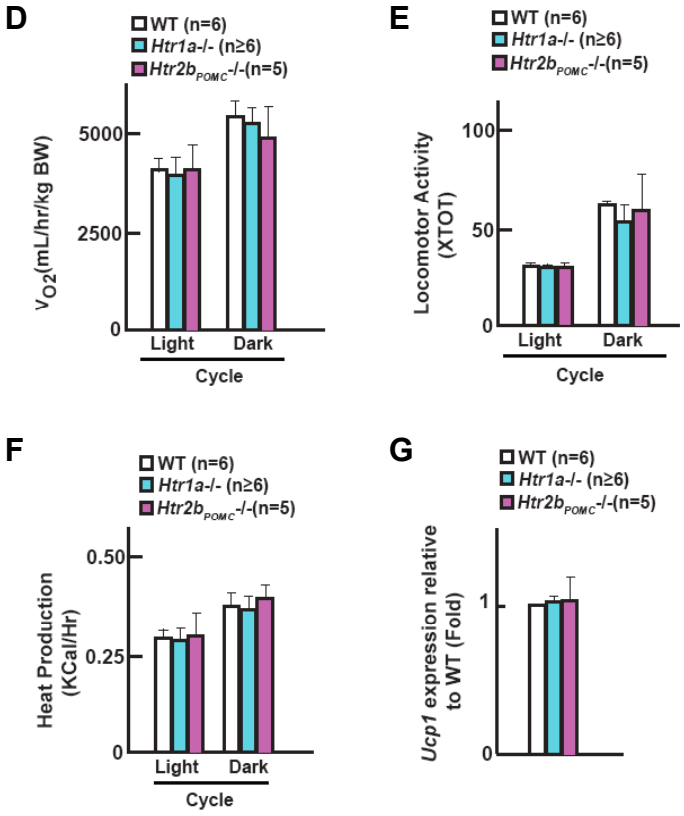

Figure S6. Volume of O_2 consumption (D), locomoter activity (E), heat production (F) and *Ucp1* expression (G) in WT, *Htr1a*-/- and *Htr2b*$_{POMC}$-/- mice.

Figure S6H. Body weight curve in *Tph2*-/- mice

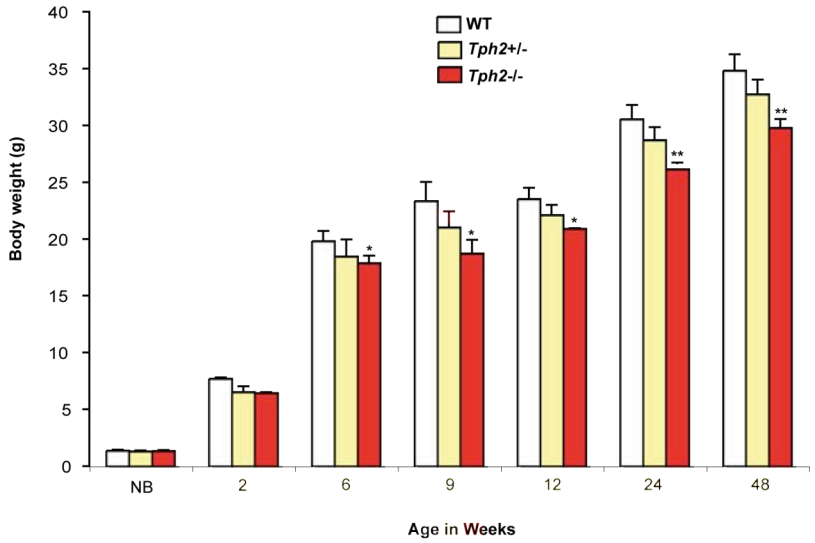

Figure S6H. Body weight curve for *Tph2* mice. WT, *Tph2*+/- and *Tph2*-/- mice were fed regular rodent chow and weighed at indicated time points. * $p<0.05$, **$p<0.01$, ***$p<0.001$ Error bars, SEM.

Figure S7. In situ hybridization analysis in *ObRb* deletion in different regions of brain

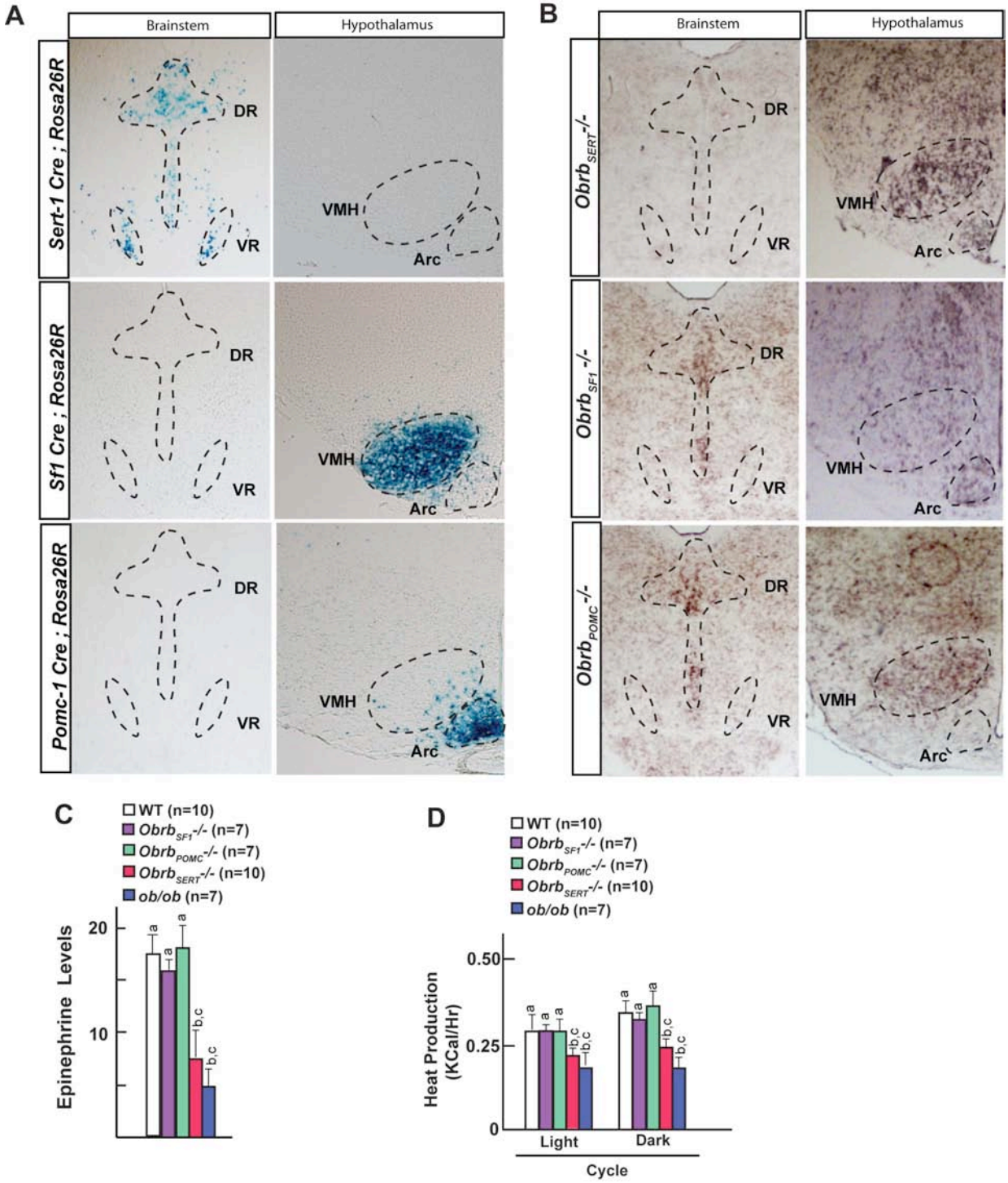

Figure S7. Specificity of *Cre* drivers and analysis of cell-specific deletion of leptin receptor (A-B). Coronal sections through Dorsal and Median Raphe (DR and MR) nuclei, and ventromedial hypothalamus (VMH) and Arcuate (ARC) nuclei (outlined by dashed lines) in adult mice. (A) β-galactosidase staining in *Sert-Cre*;*Rosa26R*, *Sf1-Cre*;*Rosa26R* and *Pomc-Cre*;*Rosa26R* mice. (B) In situ hybridization with *ObRb* probe in $ObRb_{SERT}$-/-, $ObRb_{SF1}$-/-, $ObRb_{POMC}$-/- mice. Epinephrine levels in the urine (C) and Heat production (B) in WT, $Obrb_{SF1}$-/-, $Obrb_{POMC}$-/-, $Obrb_{SERT}$-/- and *ob*/*ob* mice.

Figure S7E. Body weight curve for *ObRb* deletion in different regions of brain

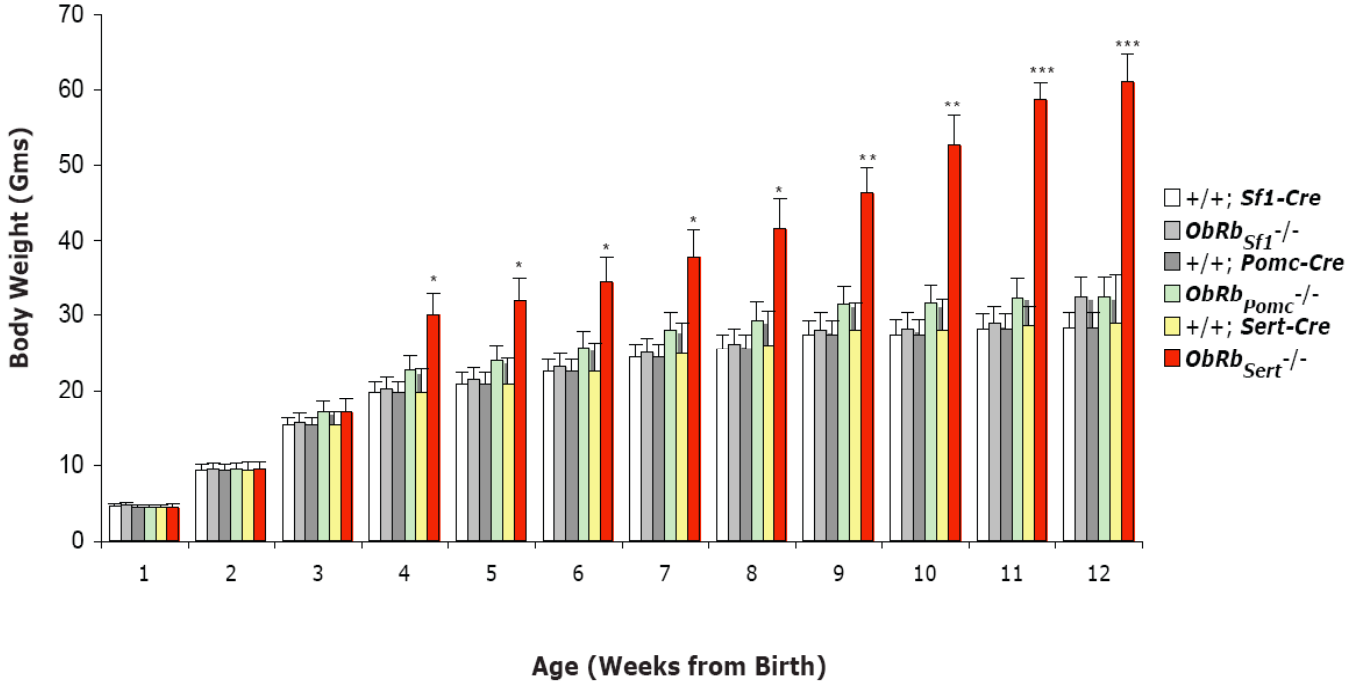

Figure S7E. Body weight curve for *ObRb* deletion in different nuclei in the brain. WT, +/+;*Sf1-Cre*, +/+;*Pomc-Cre*, +/+;*Sert-Cre, Obrb*$_{SF1}$-/-, *Obrb*$_{POMC}$-/- and *Obrb*$_{SERT}$-/- mice were fed regular rodent chow and weighed once a week. There was no significant difference in the body weights between WT, +/+;*Sf1-Cre*, +/+;*Pomc-Cre* and +/+;*Sert-Cre* mice. * $p<0.05$, **$p<0.01$, ***$p<0.001$ Error bars, SEM.

Figure 7F-G. Glucose metabolism in *ObRb$_{SERT}$*-/- mice

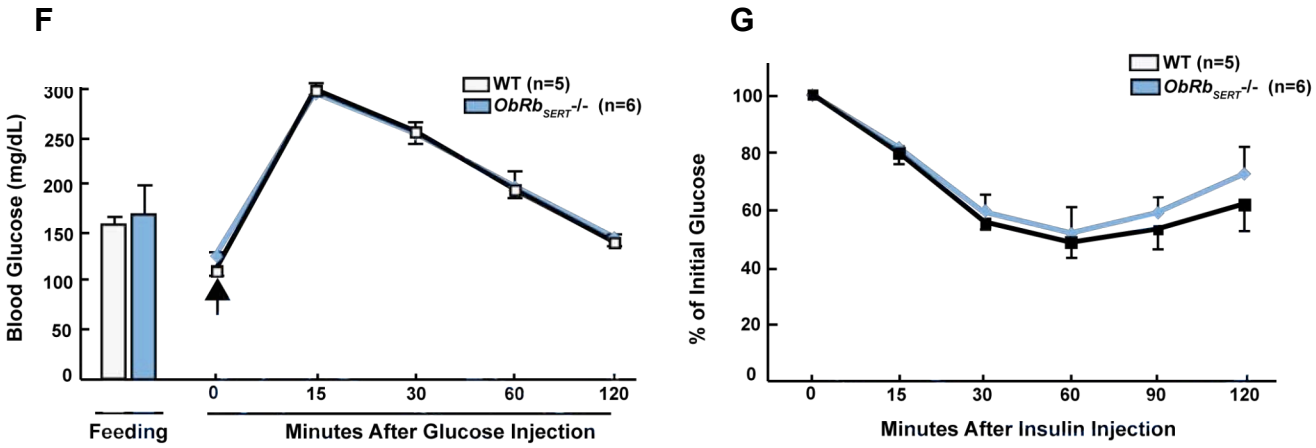

Figure S7F-G. Feeding blood glucose levels (F) Glucose tolerance (F) and insulin tolerance (G) tests in 3-month-old WT and *ObRb$_{SERT}$*-/- mice.

Figure S7H. Serum levels of T4 and Corticosterone in *ObRb$_{SERT}$*-/- mice

	WT	*ObRb$_{SERT}$*-/-	*ob/ob*
Serum T4 (ug/dL)	2.87 ± 0.12$^{(n=5)}$	3.12 ± 0.08$^{(n=5)}$	N.D.
Serum Corticosterone (ng/ml)	206.99 ± 96.43$^{(n=6)}$	176.59 ± 52.30$^{(n=5)}$	908.22 ± 167.33$^{(n=6)}$

Figure S7H. Serum T4 and corticosterone were measured by radio-immunoassay in *ObRb$_{SERT}$*-/- mice following manufacturers instructions (MP Biomedicals, Corticosterone: Cat#07-120102; T4: Cat#06B-254011)

Figure S7I. Bone mineralization is normal in *ObRb$_{SERT}$*-/- mice.

	WT	*ObRb$_{SERT}$*-/-
BV/TV%	15.29 ± 0.02$^{(n=6)}$	23.90 ± 1.31$^{(n=7)}$ *
OS/BS	17.17 ± 1.09$^{(n=6)}$	18.12 ± 1.1$^{(n=7)}$

Figure S7I. Analysis of non-mineralized bone matrix in *ObRb$_{SERT}$*-/- mice. Osteoid surface/ bone surface was measured as an indicator of changes in bone mineralization using the osteomeasure software. Data are presented as Mean ± SEM. * $p<0.05$. Student's t test.

Figure S8. Changes in *Cart* and *Tph2* expression brain

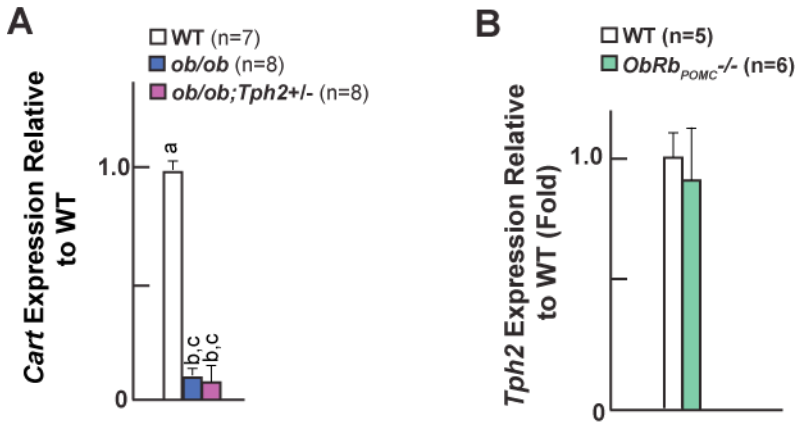

Figure S8. Real-time PCR analysis of *Cart* expression in hypothalamus in WT, ob/ob and *ob*/*ob*;*Tph2*+/- mice at 3 months of age (A). (B) Real-time PCR analysis of *Tph2* expression in brainstem in WT and *ObRb*$_{POMC}$-/- mice. $p<0.05$, SEM

Figure S9. *Htr2c* expression in the hypothalamus

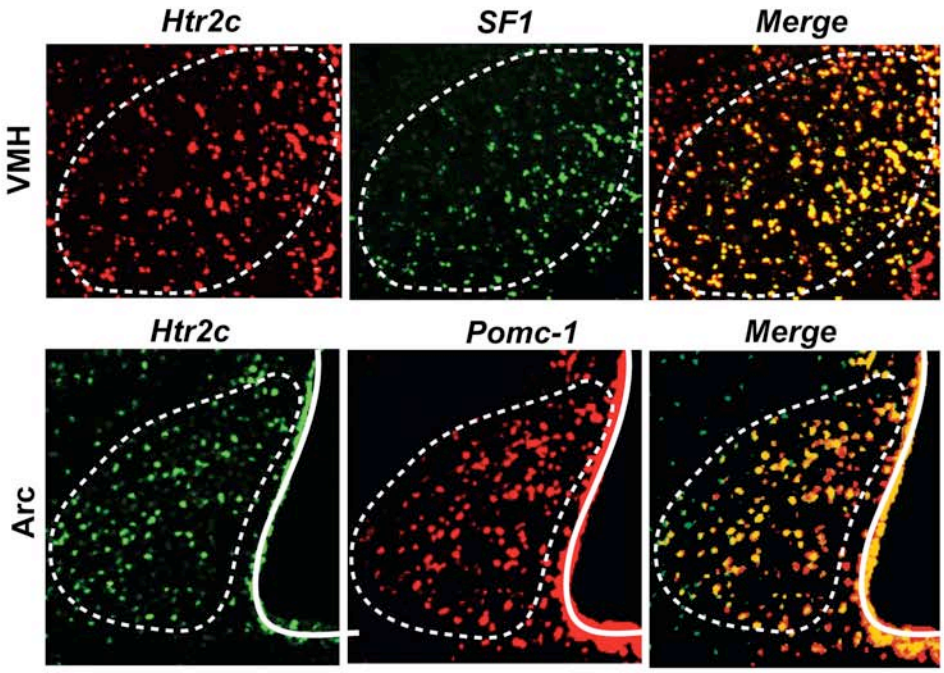

Figure S9. High magnification images of Figure 4E in situ hybridization analysis of *Htr2c, Sf1* and *Pomc* expression in ventromedial and arcuate hypothalamus**.**

Figure S10. Specificity of ObRb antibody

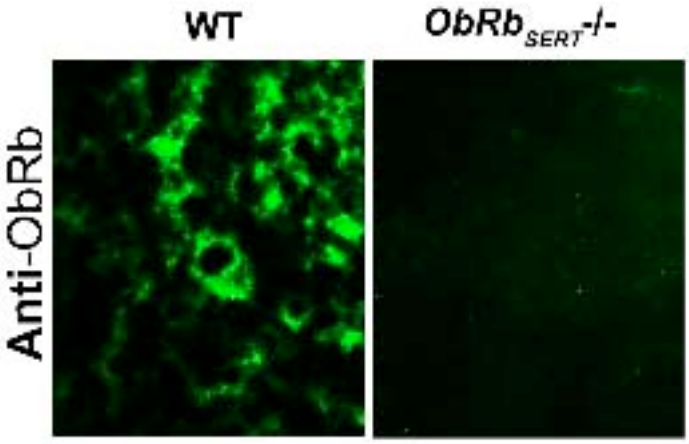

Figure S10. Immunohistochemical localization of ObRb in dorsal raphe neurons of WT and *ObRb*$_{SERT}$-/- mice.

Figure S11. *Mc4r* expression in the hypothalamus

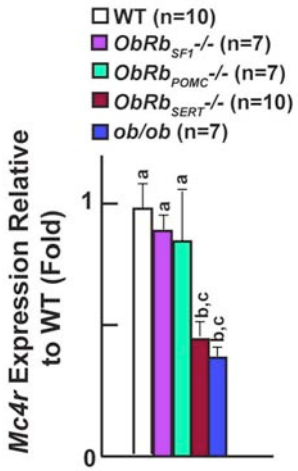

Figure S11. Real-time PCR analysis of Mc4r expression in the hypothalamus of WT, *ObRb*$_{SF1}$-/-, *ObRb*$_{POMC}$-/-, *ObRb*$_{SERT}$-/- and *ob*/*ob* mice.

Supplemental Methods:

Western blot analysis

Frozen hypoyhalamus samples were homogenized in the in 200–500 µl of RIPA buffer (10 mM NaPO4, pH 7.0, 150 mM NaCl, 2 mM EDTA, 1% sodium deoxycholate, 1% NP-40, 0.1% SDS, 50 mM NaF, 200 mM Na3VO4, 0.1% ß-mercaptoethanol, 1 mM PMSF, 4 µg/ml aprotinin, and 2 µg/ml leupeptin), and incubated on ice for 10 min with intermittent mixing before centrifugation at 15,000 x g for 10 min at 4°C. The clarified lysate was recovered, aliquoted, and stored at -80°C. For western blot analysis different amount of proteins were resolved by 10% SDS-PAGE and electroblotted onto nitrocellulose/ PVDF membrane using a wet transfer unit (Bio-Rad Laboratories, Richmond, CA). Nonspecific sites on the membrane were blocked using 10% BSA in TBST (20 mM Tris-HCl, pH 7.6, 150 mM NaCl, 0.1% Tween-20) by incubating overnight at 4°C. The membrane was then washed extensively in 1x TBST (three times for 5 min each at room temperature) and incubated at room temperature with primary antibodies (SantaCruz biotechnology Inc.) specific for different proteins [1:200 for Htr2c (sc-17797), 1:100 for Htr2b (sc-15080) and 1:100 for Htr1a (sc-10801) in TBST containing 5% BSA] for 3 h at room temperature. Secondary antibodies (horseradish peroxidase labeled anti-rabbit/ anti-goat/ anti-mouse IgG) were used at 1:2500 dilution in TBST containing 5% BSA. The bands were then visualized using an ECL kit (NEN Life Sciences).

Double immunofluorescence analysis on brain slices with pSTAT3:βGal; Tph2:ObRb and Tph2:βGal

Animals were anaesthetized and placed on a stereotaxic instrument (Stoelting) and the depth of anesthesia was determined by the animal's respiratory pattern and by pinching the animal's foot for reflex response. The dorsal part of the animal's head was shaved and prepped with betadine scrub, and 70% alcohol. The skin covering the head was then cut (approximately a 1 cm incision) and the calvaria exposed. A hole was drilled upon bregma using a 28-gauge needle. A 28 gauze needle canula (Brain infusion kit II, Alzet) was then implanted into the hole reaching the third cerebral ventricle according to the following coordinates: midline, -0.3 AP. 3mm ventral (0 point Bregma). Using a hamilton syringe, PBS or leptin (2 µg) was injected into the 3rd cerebral ventricle. The dorsal edges of the incision was coated with Bupivicaine 0.25% (< 2 mg/kg), joined and closed with 2 sterile clips. One hour later mice were anesthetized and perfused transcardially with ice-cold saline followed by 10% neutral buffered formalin. Brains were removed and postfixed for 4 hr and then cryoprotected by overnight immersion in a 20% sucrose solution. Frozen brains

were sliced in 25 μm coronal sections using a cryotome and sections were stored at -80^{0}C till utilized. For pSTAT3:βGal double immunofluorescence analysis, sections were dried at room temperature for 20 minutes pretreated with 1% NaOH, 1% H_2O_2 (20min), 0.3% glycine (10min), 0.03% SDS (10 min), blocked in donkey serum, and then incubated in rabbit pSTAT3 (tyr705) antibody (1:100, Cell Signal Technology) and chicken βGal antibody (1:500, abcam) for 24hr at 4°C. Sections were rinsed and incubated with a donkey anti-rabbit antibody (1:1000; Vector Laboratories) and donkey anti-chicken antibody (Cy3; Jackson immunoresearch).

For Tph2:βGal, 25μm coronal sections were dried at room temperature, washed with PBS, blocked in donkey serum for 1h and incubated with chicken βGal antibody (1:500 dilution, abcm) or rabbit Tph2 antibody (1:2,500 dilution) or goat ObRb antibody (1:50 dilution, Santacruz biotechnology). Sections were rinsed and incubated with donkey anti-chicken antibody (Cy3, Jackson immunoresearch) or donkey anti-goat antibody (Cy2, Jackson immunoresearch) or donkey anti-rabbit antibody (Cy2, Jackson immunoresearch).

Following staining procedures sections were mounted and coverslipped with aqueous anti-fade mounting medium for fluorescence. Staining was visualized and captured using a Zeiss fluorescent microscope.

Melanocortin sensitivity analysis

To analyze changes in melanocortin sensitivity in *Tph2*-/- mice, MTII (2ug) or saline was administered (ICV) into WT and *Tph2*-/- mice. 3 hours later mice were transcardially perfused with 4% PFA, brains were dissected and postfixed in 4% PFA overnight at 4^{0}C. Foolowing cryoprotection in 20% sucrose brains were coronally sectioned at 30um thickness. For colorimetric cFos immunohistochemistry sections were incubated for 16hrs at 4^{0}C in rabbit anti-cFos antiserum (Ab-5; 1:3000 dilution; Calbiochem), incubated with biotinylated goat anti-rabbit IgG secondary antiserum (1:600; Vector laboratories) for 2h at room temperature and then incubated in avidin biotin complex (Vector Labs). Color was developed using Vector ABC kit.

Double fluorescent in situ hybridization

Cryosections were incubated with DIG-labelled 5-HT2c receptor (5-HT2cR) cRNA probe and FITC-labelled Sf1-specific or FITC-labelled 5-HT2c receptor (5-HT2cR) cRNA probe and DIG-labelled Pomc-

specific cRNA. After stringent wash, sections were incubated with horseradish peroxidase (HRP)-conjugated anti-DIG antibody (1:1000) and labelled with Cy3 by using tyramide signal amplification (TSA) system (NEL744, PerkinElmer, USA). Followed by quenching with 1% H_2O_2, sections were incubated with HRP-conjugated anti-FITC antibody (1:1500) and labelled with FITC by TSA system (NEL741). Sections following staining were mounted in antifade mounting medium and visualized using Leica fluorescent microscope.

Metabolic Tests

Metabolic tests were performed at 2 months of age in WT, *Tph2*-/- and $ObRb_{SERT}$-/- mice following previously published procedures (Lee et al., 2007). Briefly, glucose tolerance tests (GTT) were performed after 6 hours fasting. 1 grams/kg of glucose was administrated in mice through an i.p. injection, and blood glucose was measured at 0, 15, 30, 60 and 120 minutes using Accu-check glucometer (Roche). Insulin tolerance tests (ITT) were performed after 6 hours of fasting: insulin (Sigma; 0.5 units/kg) was injected i.p., and blood glucose was measured at 0, 15, 30, 60, 90 and 120 minutes. Feeding glucose levels were measured in the morning on the mice with ad libitum access to food and water.

Electrophysiology

Brain slice preparation and electrophysiological recordings were performed as reported previously (Rao et al., 2007; Rao et al., 2008). Briefly, WT and $ObRb_{SERT}$-/- mice were anesthetized with ether and then decapitated. The brains were rapidly removed and immersed in an oxygenated bath solution at 4^0C containing (in mM): sucrose 220, KCl 2.5, $CaCl_2$ 1, $MgCl_2$ 6, NaH_2PO_4 1.25, $NaHCO_3$ 26, and glucose 10, pH 7.3 with NaOH. Coronal slices (350 μm thick) containing dorsal raphe (DR) were cut on a vibratome and maintained in a holding chamber with artificial cerebrospinal fluid (ACSF) (bubbled with 5% CO2 and 95% O_2) containing (in mM): NaCl 124, KCl 3, $CaCl_2$ 2, $MgCl_2$ 2, NaH2PO4 1.23, NaHCO3 26, glucose 10, pH 7.4 with NaOH, and were transferred to a recording chamber constantly perfused with bath solution (33^0C) at 2 ml/min after at least a 1 hr recovery.

Whole-cell current clamp was performed to observe action potentials in DR serotoninergic (5-HT) neurons with a Multiclamp 700A amplifier (Axon instrument, CA). The patch pipettes with a tip resistance of 4-6

MΩ were made of borosilicate glass (World Precision Instruments) with a Sutter pipette puller (P-97) and filled with a pipette solution containing (in mM): K-gluconate (or Cs-gluconate) 135, $MgCl_2$ 2, HEPES 10, EGTA 1.1, Mg-ATP 2, Na_2-phosphocreatine 10, and Na_2-GTP 0.3, pH 7.3 with KOH. After a giga-Ohm (GΩ) seal and whole-cell access were achieved, the series resistance (between 20 and 40 MΩ) was partially compensated by the amplifier. 5-HT neurons were identified according to their unique properties (long-duration action potential, activation by norepinephrine and inhibition by serotonin itself) reported previously (Liu et al., 2002). Under current clamp, 5-HT neurons were usually quiescent in slices because of the loss of noradrenergic inputs. The application of α1-adrenergic agonist phenylephrine (PE, 3 μM) elicited action potentials and the application of serotonin creatinine sulfate complex (3 μM) inhibited action potentials in these neurons. The effect of leptin on 5-HT neurons was examined in DR neurons responding to both PE and serotonin. Before the application of leptin, action potentials in 5-HT neurons were restored by application of PE in the bath (Liu et al., 2002). All data were sampled at 3-10 kHz and filtered at 1-3 kHz with an Apple Macintosh computer using Axograph 4.9 (Axon Instruments). Electrophysiological data were analyzed with Axograph 4.9 and plotted with Igor Pro software (WaveMetrics, Lake Oswego, OR).

Rhodamine-conjugated dextrans labeling

Rhodamine-conjugated dextrans (Molecular Probes, Eugene, Oregonaxonal) were used as axonal tracers in an ex vivo preparation. These substances are efficiently taken up by injured axons and transported rapidly along the axonal structure anterogradely to the axonal terminals and retrogradely to the cell bodies. We employed anterograde and retrograde labeling respectively for the staining of axonal projections of the Median Raphe nuclei (MR) and axonal projections reaching the VMH and Arcuate nuclei as previously described (Oury et al., 2006) with the following modifications. Axonal projection of the MR nuclei were labeled by applying dextran crystals in a surgically created pouch in *Tph2LacZ*/+ mice (P0-P4). The surgical application of dextran was confirmed by comparison on section after β-galactosidase staining visualizing the serotonergic neurons. Axonal tracing of the projections reaching the VMH and Arcuate nuclei were performed in *Sf1-Cre*;*Rosa26R* and *Pomc-Cre*;*Rosa26R* mice respectively and realized in *Tph2LacZ*/+ mice by applying dextran crystals in the hypothalamus between the pituitary gland and the optic chiasm. The surgical application of dextran was confirmed by comparison on section after β-galactosidase staining. After the fluorescent-dextran crystal application, the brains were maintained alive in the oxygenated physiological

saline liquid as described (Oury et al., 2006). After up to 16 hours of postoperative incubation, the brains were fixed in buffered 4% paraformaldehyde overnight at 4°C and embedded into 3% agarose. All preparations were sectioned on a vibratome at 200 μm (Figure 4B-C and 6F) or 50 μm (Figure S4A) and analyzed under microscope (Leica).

β-Galactosidase staining

β-Galactosidase staining was performed on the tissues obtained from the *Tph2*+/- mice following standard procedures. Briefly, tissue samples were dissected after intracardial perfusion with ice-cold 4% paraformaldehyde in PBS, and fixed for 1-2 h. The samples were then washed three times with washing buffer (0.2% Nonidet P-40, 0.1% sodium deoxycholate, 100 mM phosphate buffer (pH 7.4), 2 mM magnesium chloride) for 15–30 min each and then stained at 37°C overnight (12–16 h) in freshly prepared LacZ-staining solution containing 0.2% Nonidet P-40, 0.1% sodium deoxycholate, 100 mM phosphate buffer (pH 7.4), 2 mM magnesium chloride, 3 mM potassium ferricyanide, 3 mM potassium ferrocyanide, and 0.5 mg/ml X-gal (5-bromo-4-chloro-3-indolyl-D-galactopyranoside) protected from light. After the staining overnight tissues were photographed before processing them for paraffin embedding for histology. Paraffin blocks were sectioned at 5-7 μm thickness, deparaffinized and counterstained with eosin, cleared in xylene and mounted in DPX.

μCT analysis

Trabecular bone architecture of distal tibia was assessed using a micro computed tomography (μCT) system (VivaCT 40, SCANCO Medical AG, Switzerland). Tibial bone specimen was stabilized with gauze in a 2 ml centrifuge tube filled with 70% ethanol and fastened in the specimen holder of the μCT scanner. One hundred μCT slices, corresponding to a 1.05 mm region distal from the growth plate, were acquired at an isotropic spatial resolution of 10.5 μm. A global threshold technique was applied to binarize gray-scale μCT images where the minimum between the bone and bone marrow peaks in the voxel gray value histogram was chosen as the threshold value. The trabecular bone compartment was segmented by a semi-automatic contouring method and subjected to a model-independent morphological analysis (Hildebrand et al., 1999) by the standard software provided by the manufacturer of the μCT scanner. 3D morphological parameters, including bone volume fraction (BV/TV), Tb.Th. (trabecular thickness), and connectivity density (Conn.D)

were evaluated. The Conn.D is a quantitative description of the trabecular connection (Feldkamp et al., 1989; Gundersen et al., 1993).

Physiological measurements

For food intake studies, mice were individually housed in metabolic cage (Nalgene, Rochester, NY) and fed ad libitum. Food consumption amount was determined by weighing the powdered chow before and after the 24-hour measurement. Oxygen consumption (V_{O2}) and respiratory exchange ratio (RER) were measured by indirect calorimetry method using a six-chamber Oxymax system (Columbus Instruments, Ohio). Mice were individually housed in the chamber and fed ad libitum. After 30-hour acclimation to the apparatus, data for 24-hour measurement were collected and analyzed as recommended by the manufacturers of the energy expenditure apparatus (Columbus Instruments, Ohio).

Bone histomorphometric analyses

Bone histomorphometry was performed as previously described (Baron et al., 1983; Chappard et al., 1987; Parfitt et al., 1987). Briefly, lumbar vertebrae were dissected, fixed for 24 hr in 10% formalin, dehydrated in graded ethanol series, and embedded in methyl methacrylate resin according to standard protocols. Von Kossa/Von Gieson staining was performed using 7 μm sections for bone volume over tissue volume (BV/TV) measurement. Bone formation rate (BFR) was analyzed by the calcein double-labeling method. Calcein (Sigma Chemical Co., St. Louis, MO) was dissolved in calcein buffer (0.15 M NaCl, 2% NaHCO3) and injected twice at 0.125 mg/g body weight on day 1 and 4, and then mice were killed on day 6. Four μm sections were cleared in xylene and used for bone formation rate (BFR) measurements. For the analysis of parameters of osteoblast and osteoclast, 4 μm sections were stained with toluidine blue and tartrate-resistant acid phosphatase (TRAP) respectively. Histomorphometric analyses were performed using the Osteomeasure Analysis System (Osteometrics, Atlanta, GA).

References

Baron, R., Vignery, A., Neff, L., Silvergate, A., and Maria, A.S. (1983). Processing of undecalcified bone specimen for bone histomorphometry. In Bone histomorphometry: techniques and interpretation, R.R. Recker, ed. (Boca raton, CRC press), pp. 13-25.

Chappard, D., Palle, S., Alexandre, C., Vico, L., and Riffat, G. (1987). Bone embedding in pure methyl methacrylate at low temperature preserves enzyme activities. Acta Histochem *81*, 183-190.

Feldkamp, L.A., Goldstein, S.A., Parfitt, A.M., Jesion, G., and Kleerekoper, M. (1989). The direct examination of three-dimensional bone architecture in vitro by computed tomography. J Bone Miner Res *4*, 3-11.
Gundersen, H.J., Boyce, R.W., Nyengaard, J.R., and Odgaard, A. (1993). The Conneulor: unbiased estimation of connectivity using physical disectors under projection. Bone *14*, 217-222.
Hildebrand, T., Laib, A., Muller, R., Dequeker, J., and Ruegsegger, P. (1999). Direct three-dimensional morphometric analysis of human cancellous bone: microstructural data from spine, femur, iliac crest, and calcaneus. J Bone Miner Res *14*, 1167-1174.
Lee, N.K., Sowa, H., Hinoi, E., Ferron, M., Ahn, J.D., Confavreux, C., Dacquin, R., Mee, P.J., McKee, M.D., Jung, D.Y*., et al.* (2007). Endocrine regulation of energy metabolism by the skeleton. Cell *130*, 456-469.
Liu, R.J., van den Pol, A.N., and Aghajanian, G.K. (2002). Hypocretins (orexins) regulate serotonin neurons in the dorsal raphe nucleus by excitatory direct and inhibitory indirect actions. J Neurosci *22*, 9453-9464.
Oury, F., Murakami, Y., Renaud, J.S., Pasqualetti, M., Charnay, P., Ren, S.Y., and Rijli, F.M. (2006). Hoxa2- and rhombomere-dependent development of the mouse facial somatosensory map. Science *313*, 1408-1413.
Parfitt, A.M., Simon, L.S., Villanueva, A.R., and Krane, S.M. (1987). Procollagen type I carboxy-terminal extension peptide in serum as a marker of collagen biosynthesis in bone. Correlation with Iliac bone formation rates and comparison with total alkaline phosphatase. J Bone Miner Res *2*, 427-436.
Rao, Y., Liu, Z.W., Borok, E., Rabenstein, R.L., Shanabrough, M., Lu, M., Picciotto, M.R., Horvath, T.L., and Gao, X.B. (2007). Prolonged wakefulness induces experience-dependent synaptic plasticity in mouse hypocretin/orexin neurons. J Clin Invest *117*, 4022-4033.
Rao, Y., Lu, M., Ge, F., Marsh, D.J., Qian, S., Wang, A.H., Picciotto, M.R., and Gao, X.B. (2008). Regulation of synaptic efficacy in hypocretin/orexin-containing neurons by melanin concentrating hormone in the lateral hypothalamus. J Neurosci *28*, 9101-9110.